CrossMark

Mesostructure optimization in multi-material additive manufacturing: a theoretical perspective

Hang Z. Yu[1,2,*], Samuel R. Cross[1,3], and Christopher A. Schuh[1,*]

[1]Department of Materials Science and Engineering, Massachusetts Institute of Technology, Cambridge, MA 02139, USA
[2]Present address: Department of Materials Science and Engineering, Virginia Tech, Blacksburg, VA 24061, USA
[3]Present address: Xtalic Corporation, 260 Cedar Hill Street, Marlborough, MA 01752, USA

ABSTRACT

As multi-material additive manufacturing technologies mature, a new opportunity for materials science and engineering emerges between the scale of the microstructure and the scale of an engineering component. Here we explore the problem of "mesostructure optimization," the *computational identification* of preferred point-to-point distributions of material structure and properties. We illustrate the opportunity with two simple example problems for 1D and 2D mesostructure optimization, respectively, namely (1) a functionally graded cylinder that is computationally optimized to redistribute the Hertzian contact stress fields and (2) a thin plate made of digital materials computationally designed to simultaneously maximize bending resistance and minimize total weight. The mechanical performance of materials in these two problems is significantly improved as compared to any monolithic-material counterpart, including a topology-optimized monolith in case (2). These results point to new opportunities for multi-objective performance enhancement in materials.

Introduction

Additive manufacturing offers unique capabilities that are unavailable from traditional casting, working, or machining-based manufacturing methods, and is therefore dramatically influencing a wide variety of industries [1–4]. One of the most celebrated capabilities of additive manufacturing so far is the ability to render complex shapes in three dimensions [5–7]. From the perspective of a materials scientist or materials engineer, however, an even greater potential is offered by the possibility of point-wise control over material structure, i.e., the mesoscale distribution of material composition, microstructure, and properties across an entire component. In structural and thermal applications, the stress and thermal fields are often highly non-uniform; control of mesostructure can simultaneously locate different properties at different positions of the component for optimum overall performance.

Based on the technological trajectory of 3D printing or additive manufacturing, mesostructure control is expected to be available for a wide variety of materials within a few years. For instance, by delivering a

mixture of multiple materials as the feedstock and by varying the volume ratio of each material during the rapid solidification or curing process, 3D objects with controlled composition and property gradients have been demonstrated in metal alloys using directed energy deposition [8, 9] and in polymers using inkjet-based 3D printing [10]. Such "multi-material" additive manufacturing processes allow for control of the material mesostructure and the 3D geometry simultaneously, unlocking the possibility of materials design and optimization across multiple length scales.

However, the vast freedom of the materials design space also demands that we learn to optimize across it: what is the optimum component when every voxel of material can have tuned composition and properties? The optimal geometry of a component can already be computationally determined via topology optimization [11–19], usually assuming a monolithic material. Similarly, while microstructure optimization strategies abound in the field of materials science [20–23], these are generally not applied as a function of position across the scale of a component and are generally targeted at statistically homogeneous materials [22]. As illustrated in Fig. 1, the field that lies between topology optimization and microstructure optimization is mesostructure optimization—an area decidedly enabled by the prospect of multi-material additive manufacturing. Our purpose in this paper is to computationally explore some possibilities in this area.
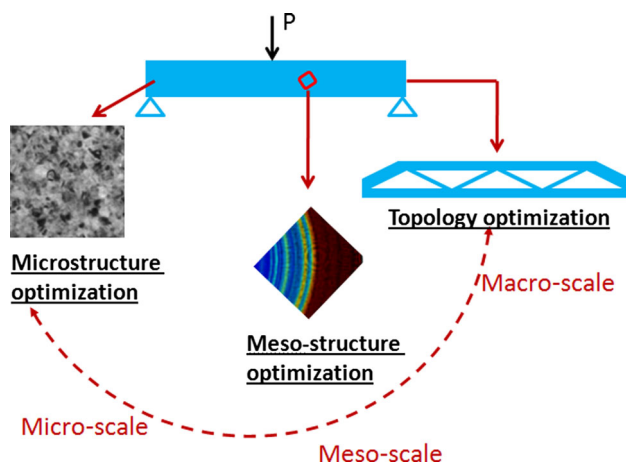
Figure 1 Illustration of optimization at the macroscale (topology optimization), microscale (microstructure optimization) and mesoscale (mesostructure optimization).

Mesostructure optimization in Hertzian contact

The basic algorithms used widely for optimizations of all kinds [11–23] should generally be applicable to the mesostructure optimization problem, and those methods used in topology optimization should be particularly portable. Optimization of material mesostructure has been addressed with such techniques in some narrow domains in the past. For example, Cross et al. [24] have addressed galvanic corrosion problems through optimization of compositionally graded coatings for cathodic protection. In fact, the field of functional gradient materials [25–27] is one in which a gradient is widely appreciated as providing a preferred solution to any monolithic alternative, but to our knowledge formal optimization of the shape of the gradient structure has not been undertaken. From our perspective, optimal gradient materials are a natural starting point toward full component mesostructure optimization.

Problem statement

As an illustration, consider a Hertzian contact problem: a long cylinder is elastically compressed by two steel blocks with frictionless contact (see Fig. 2a). The steel blocks have fixed and homogeneous elastic properties, while the cylinder will be fabricated using a multi-material additive manufacturing technology with controlled mesoscale distribution of elastic properties. For simplicity, we limit our consideration to axially symmetric cylinders, so that the cylinder is, in fact, a radially graded material. The cylinder is susceptible to shear yield, and for a monolithic material, the Hertzian elastic equations [28] provide a basis to understand its mechanical limits. Once the mesostructure is viewed as tunable, however, the stress fields in a loaded cylinder are no longer restricted to the Hertzian solutions and can be "sculpted" by introducing a spatially dependent elastic (and plastic) property field.

The goal of an optimization exercise is then to answer questions of the following type: under a set of physical constraints, e.g., for a fixed cylinder radius R and applied load F, and given a certain range of internal properties accessible in manufacturing the component (e.g., Young's modulus E and Poisson's ratio v).
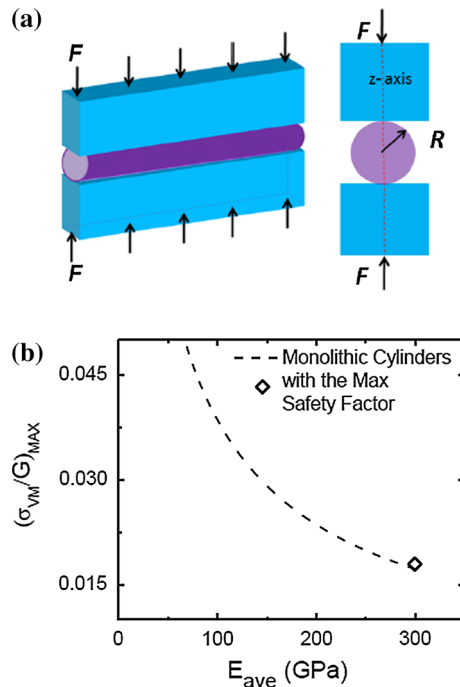
Figure 2 a Illustration of the Hertzian contact problem studied in this work. **b** Plot of the objective function $(\sigma_{\text{VM}}/G)_{\text{max}}$ as a function of Young's modulus E for monolithic cylinders.

- What is the maximum safety factor against mechanical overload or the minimum failure risk of the cylinder?
- What is the minimum contact area or the minimum degree of deformation of the cylinder?
- For a given limiting acceptable contact area or for a given degree of deformation, what is the lowest achievable weight of the cylinder?

As an illustrative example, we employ the following set of constraints in a first calculation for the maximum safety factor against mechanical overload of the cylinder. Using a von Mises yield criterion, the first yield occurs when the local von Mises stress exceeds the local strength at any point of the cylinder. The failure criterion can thus be written as $\left(\frac{\text{Local von Mises Stress}}{\text{Local Strength}}\right)_{\text{max}} \geq 1$, where the subscript "max" denotes the maximum value at any point within the cylinder. To minimize the risk of mechanical failure or maximize the safety factor against mechanical overload, our task is to minimize the value of $\left(\frac{\text{Local von Mises Stress}}{\text{Local Strength}}\right)_{\text{max}}$.

The local strength of a mesostructured material is dependent on the local material composition, microstructure, and elastic properties. Here we take

the strength of the local material to scale with the local shear modulus, so that the first yield occurs when $\left(\frac{\text{Local von Mises Stress}}{\text{Local Shear Modulus}}\right)_{\text{max}}$ exceeds a critical value, i.e., when $(\sigma_{\text{VM}}/G)_{\text{max}} \geq \gamma_c$. σ_{VM} denotes the von Mises stress, G is the shear modulus, and the dimensionless constant γ_c is a measure of the yield strain. It should be noted that this arbitrary assumption of yield criterion is for calculation purposes only and has its limits; a practical optimization problem would require measurement of the yield strength as a function of the material composition to determine the yield criterion. The safety factor against mechanical overload of a mesostructured cylinder can then be defined as $X = \frac{\gamma_c}{(\sigma_{\text{VM}}/G)_{\text{max}}}$. For cylinders with different mesostructures, the safety factor X is maximized when the value of $(\sigma_{\text{VM}}/G)_{\text{max}}$ is minimized. Therefore, $(\sigma_{\text{VM}}/G)_{\text{max}}$ is the *objective function* of this optimization problem.

We further constrain the elastic properties and geometry of the cylinder and blocks as follows. First, the cylinder is envisioned as being fabricated using two mixable source materials, a stiff material with a Young's modulus of 300 GPa and a soft material with a Young's modulus of 3 GPa. The rule of mixture at the voxel level follows the simple Voigt model [29]. By mixing these two materials and controlling their volume ratios during the additive manufacturing process, the Young's modulus E can be tuned from 3 to 300 GPa at any point within the cylinder. In addition, the steel blocks are taken to have a Young's modulus $E_{\text{block}} = 200$ GPa, and both the cylinder and block have a Poisson's ratio $v = 0.3$. The radius of the cylinder is $R = 50$ mm, and the force per unit length is $F = 15$ kN/mm. The parameters used in this work are summarized in Table 1.

Monolithic cylinders

As a baseline, it is useful to consider monolithic cylinders with properties that span the allowed range (with E ranging from 3 to 300 GPa and strength varying in proportion). According to the Hertzian

Table 1 List of parameters used for computation

Cylinder: stiff material	$E_{\text{max}} = 300$ GPa	$v = 0.3$
Cylinder: soft material	$E_{\text{min}} = 3$ GPa	$v = 0.3$
Steel blocks	$E_{\text{block}} = 200$ GPa	$v = 0.3$
Force per unit length	$F = 15$ kN/mm	
Cylinder radius	$R = 50$ mm	

contact theory [28], the maximum von Mises stress in the cylinder is found along the z-axis and is close to the contact surface. With Young's modulus E and Poisson's ratio $v = 0.3$, the value of the objective function for a monolithic cylinder is

$$(\sigma_{VM}/G)_{max} = \frac{0.56}{G}\left(\frac{FE^*}{\pi R}\right)^{1/2}$$
$$= 1.12\left(\frac{F}{\pi R}\right)^{1/2}\left[\frac{E_{block}(1+v)}{E(1-v)(E+E_{block})}\right]^{1/2},$$
(1)

where E^* is defined as $\frac{1}{E^*} = \frac{1-v^2}{E} + \frac{1-v^2}{E_{block}}$. Figure 2b plots the value of $(\sigma_{VM}/G)_{max}$ as a function of E in the cylinder. The objective function is minimized when the value of E is maximized; as a result, in monolithic cylinders the maximum safety factor is achieved with the material of the maximum elastic modulus $E = 300$ GPa. The minimal value of $(\sigma_{VM}/G)_{max}$ is calculated as 0.0172, corresponding to a safety factor $X = 58.1\gamma_c$.

Mesostructured cylinders

To compute the values of $(\sigma_{VM}/G)_{max}$ for a mesostructured cylinder, finite element analysis is conducted using the COMSOL Multiphysics solver via the LiveLink for MATLAB software package. Numerical optimization is conducted using a simulated annealing algorithm [15, 16, 24, 30], with the goal of minimizing the value of $(\sigma_{VM}/G)_{max}$. During each iteration k, the simulated annealing algorithm mutates the parent distribution by addition of a random Gaussian function to the modulus distribution. Finite element analysis is then employed to compute the change in the objective function, $\Delta(\sigma_{VM}/G)_{max}$. A step that decreases the objective function value is always adopted; a step that increases the objective function value is adopted with a finite probability given by the Metropolis criterion $P = \exp(-\frac{\Delta(\sigma_{VM}/G)_{max}}{T})$, with the temperature parameter T slightly decreasing in each iteration. If the candidate distribution is accepted, it becomes the parent distribution for the next iteration $(k + 1)$. The occasional acceptance of inferior values allows the optimization algorithm to escape local minima and to move quickly through large valleys in the design space. The algorithm is run for a total of 2000 iterations. The current best distribution of Young's

modulus and the minimal value of $(\sigma_{VM}/G)_{max}$ are recorded throughout this process.

We first consider a cylinder made of ten concentric layers each of the same volume. The optimization problem can then be stated as follows:

Minimize : $(\sigma_{VM}/G)_{max}$ $(E_i, i = 1, 2, \ldots 10)$
Subject to : $3\,\text{GPa} \le E_i \le 300\,\text{GPa}$

Three separate simulations are run with different initial distributions of E_i: (1) $E_i = 300$ GPa, (2) $E_i = 151.5$ GPa, and (3) $E_i = \frac{300[1-\exp(-i/100)]}{[1-\exp(-1/10)]}$ GPa $(i = 1, 2, \ldots 10)$, to test that the outcome of the optimization is insensitive to the initial condition. Figure 3a plots the value of $(\sigma_{VM}/G)_{max}$ as a function of the iteration number for these cases, in which the optimal solution eventually converges to the same point regardless of the initial distribution of E_i in the simulation. The stochastic nature of the optimization algorithm is demonstrated in Fig. 3b, in which the path traced by a representative simulated annealing run is shown. Here E_{ave} is the volume-weighted average Young's modulus of the cylinder.

The optimal material distribution determined by the simulated annealing algorithm is shown in Fig. 3c, with the Young's modulus increasing from the center to the outer layers of the cylinder. In the ten-layer case, the optimal radial distribution of the Young's modulus is a staircase-like function, monotonically increasing in modulus toward the surface in a nonlinear fashion. The shape of this distribution is worth further discussion, but there is one aspect that is strictly an artifact of the optimization methodology: the series of abrupt changes of elastic properties within the cylinder at the (artificially defined) layer interfaces. Since material incompatibilities associated with sharp interfaces can lead to high internal stresses and strains, increase the local values of triaxiality, and promote inception of flaws [27], further optimization would involve refinement of the mesostructure. For example, when we increase the number of layers from 10 to 100, still under the restriction that the layers are concentric and all of the same volume, a smoother optimal distribution of Young's modulus is obtained, as also shown in Fig. 3c. The optimized cylinder consists of a compliant core with a radius ~ 10 mm and $E \sim 27$ GPa, a stiff shell with a thickness ~ 8 mm and $E = 300$ GPa, and an approximately 32-mm-thick transition region between the core and shell (see Fig. 3d). Following

Figure 3 **a** Plot of the objective function as a function of iteration number during simulated annealing, with the results compared for three different initial distributions. **b** Plot of the path traced by a representative simulated annealing run. **c** Optimal distribution of Young's modulus for the cases of 10 and 100 concentric layers. **d** The stiff shell, compliant core, and the transition region in the optimized cylinder.
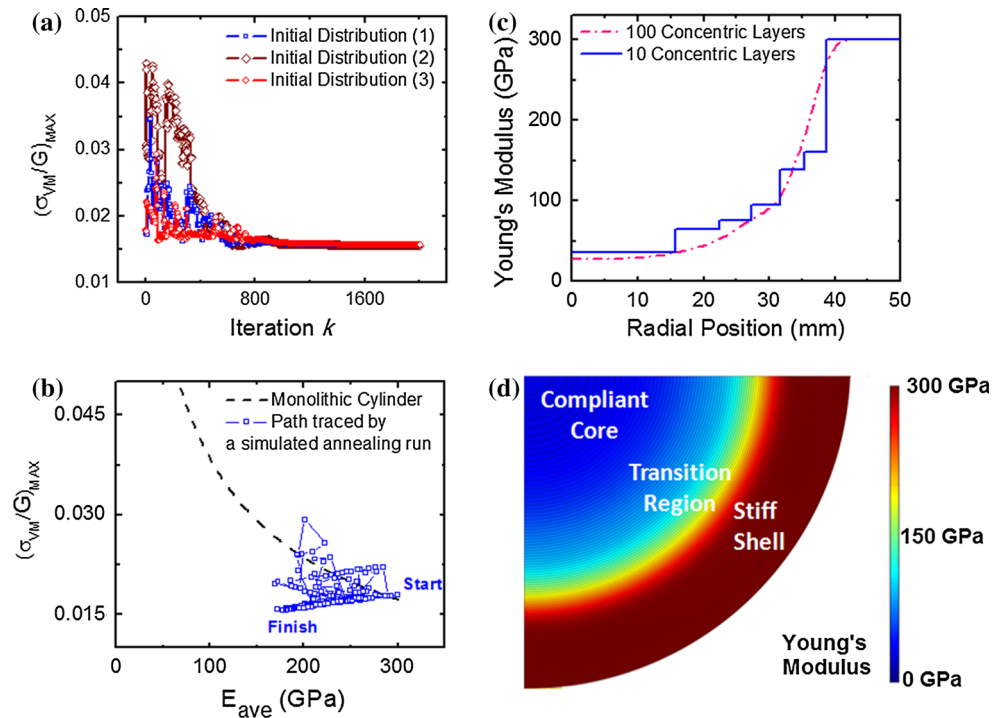
the simple Voigt model, the compliant core consists of ∼92% of the soft source material and ∼8% of the stiff source material, whereas the stiff shell is comprised entirely of the stiff source material.

The optimization results are further analyzed in Fig. 4, showing how the load path is influenced by mesoscale materials design. For the optimized cylinder, the objective function is computed as $(\sigma_{VM}/G)_{max} = 0.0148$ with $E_{ave} = 174$ GPa. This corresponds to a safety factor $X = 67.6\gamma_c$. For the monolithic cylinder with the same E_{ave} (blue square in Fig. 4), the objective function is computed as $(\sigma_{VM}/G)_{max} = 0.0263$, which corresponds to a safety factor $X = 38.0\gamma_c$. Through mesostructure optimization, therefore, the safety factor against mechanical overload is increased by 78% (from $38.0\gamma_c$ to $67.6\gamma_c$), without increasing the average Young's modulus.

It should be emphasized that the optimized cylinder has a higher safety factor against mechanical overload than all possible monolithic cylinders with properties taken from within the design set. In the latter case, the minimal objective function or the maximum safety factor is achieved in the most stiff cylinder with $E = 300$ GPa (black diamond in Fig. 4). As discussed in Sect. 2.2, this corresponds to a safety factor $X = 58.1\gamma_c$, which is still 16% lower than that of the optimized cylinder $X = 67.6\gamma_c$. In other words, even the best monolithic cylinder is less safe than the

optimal cylinder, despite having an average elastic modulus 72% higher.

The advantage of mesostructure optimization originates from its capability of reshaping the characteristic stress and strain fields involved in a mechanical problem such as this. For the monolithic stiff cylinder ($E = 300$ GPa, upper box in Fig. 4), the von Mises stress is strongly concentrated near the point of contact. For the optimized cylinder, because of the presence of the property gradient, the von Mises stress concentration is shifted away from the z-axis (highlighted using white five-pointed stars) and is distributed widely through the stiff shell (lower box in Fig. 4). This results in a lower maximum value of the von Mises stress at any point throughout the optimized cylinder. The optimized mesostructure matches the distribution of the stiff material to the areas expected to have the maximum stress, providing the ideal balance between the stress redistribution and the strength of the stiff material. As a result, the optimized cylinder has a lower value of $(\sigma_{VM}/G)_{max}$ and a higher safety factor against mechanical overload.

Comparing the two cases highlighted in Fig. 4, the safety factor X is increased from $58.1\gamma_c$ to $67.6\gamma_c$ and the value of E_{ave} is decreased from 300 to 174 GPa in the optimized cylinder. Mesostructure optimization, therefore, is capable of increasing the safety factor
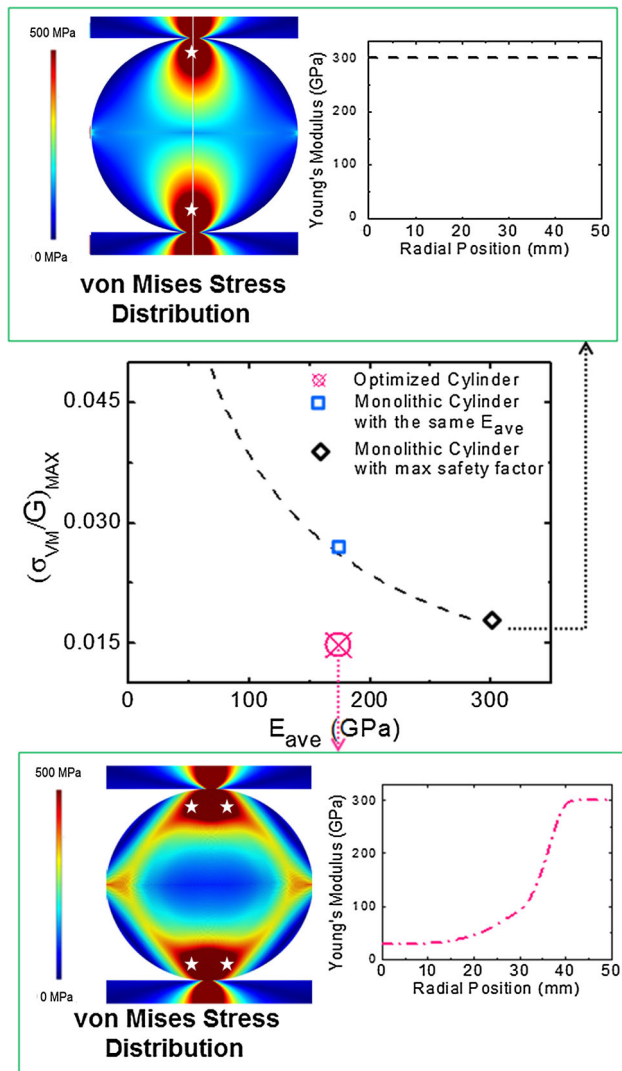
Figure 4 Plot of the objective function $(\sigma_{VM}/G)_{max}$ as a function of the average modulus E_{ave}, with the results compared for the optimized cylinder and monolithic cylinders. The von Mises stress distribution is compared for a monolithic stiff cylinder (*upper box*) and the cylinder with the optimal mesostructure (*lower box*). In both cases, the locations with maximum von Mises stress are highlighted using white five-pointed stars.

against mechanical overload and lowering the average modulus of cylinder at the same time. Although not explicitly included in the objective function used for optimization, the remarkable decrease in E_{ave} suggests that a similar approach may be applicable in design of mesostructures with the aim to simultaneously maximize load-bearing capacities and minimize the weight or cost of manufactured parts. In principle, application of these methods to other geometries and problems of interest should be

straightforward for any property amenable to finite element analysis.

The optimization results in Figs. 3 and 4 suggest an efficient way of distributing materials in cylindrical structures for mechanical applications. Interestingly, such stiff shell-compliant core design is widely observed in a variety of natural and biological structural materials. For example, the primary skeletal elements in sharks, rays, and their relatives exhibit highly mineralized, stiff outer layers (known as tesserae) at the perimeter to protect inner structures [31]. Wood and bones develop a similar gradient structure effected through relative density [32, 33]. Mesoscale material distribution in these natural and biological materials enables better mechanical performance and lower weight. We note that the optimization criteria for biological materials are far more complex than the case being considered here, where multiple "design goals," such as weight reduction, mechanical performance (contact resistance, damage localization, bending resistance, etc.), growth and health, were nominally all contributing to the evolutionary process of optimization. For engineering materials optimized to specific mechanical needs, actual instantiation of optimal mesostructures may await further advances in processing. In principle, radially graded cylinders like the one considered here should be producible using multi-material additive manufacturing technologies. For example, using laser engineered net shaping (LENS), Hofmann et al. [8] showed that a mesostructured cylinder radially graded from 304 L (inner side) to Invar 36 (outer side) can be made by depositing a mixture of the two powders on a rotating rod substrate and controlling the volume fraction during deposition. In their graded cylinder, the coefficient of thermal expansion (CTE) continuously varied from 1.6×10^{-5} to 0/K from the center to the edge, while the Young's modulus ranged from ~ 240 to ~ 160 GPa. LENS has shown great potential for fabricating components with a wide range of tunable properties and gradient structures [34–38]. By mixing TiC and Ti powders, for instance, Liu and DuPont [39] produced a graded composite with the hardness in the deposit increasing from about 200 Vickers hardness number (VHN) on the Ti side to approximately 2300 VHN at the top layer as the TiC content increased. These encouraging examples show promise of implementing mesostructure optimization

using multi-material additive manufacturing processes in the near future.

2D mesostructure optimization in a thin plate subjected to bending

Mesostructure optimization is not limited to 1D as in the above example, but can also be implemented in 2D and 3D. In this section, an example of 2D mesostructure optimization is illustrated by optimizing a thin plate subjected to three-point bending, which is relevant to lightweight applications such as sandwich panels [29].

Problem statement

As shown in Fig. 5a, a thin plate with a length $L_x = 10$ cm along the x-direction and thickness $L_z = 2$ cm along the z-direction is subjected to three-point bending. The out-of-plane width L_y along the y-direction is large, so the plate is under a plane-strain condition and can be modeled as a 2D domain. We assume that through multi-material additive manufacturing, the plate can be made with digital materials with the same range of elastic properties used in the prior example, i.e., Young's moduli ranging from 3 to 300 GPa, with a Poisson ratio fixed at 0.3. The density of each material is assumed to be proportional to the Young's modulus.

(a)
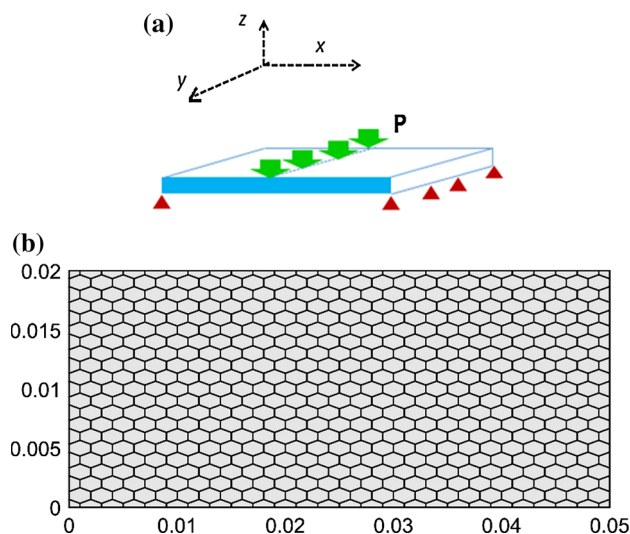
Figure 5 **a** Illustration of the 2D mesostructure optimization problem: a thin plate subjected to bending. **b** The right half of the x–z plane of the plate, which is divided into 536 hexagonal design elements.

The 2D optimization problem considered here is how to adjust the distribution of these materials in the x–z plane to simultaneously maximize the resistance to bending and minimize the total weight. Given the symmetry in this problem, we only need to analyze the right half of the 2D domain, which is divided into 536 hexagonal design elements, as shown in Fig. 5b. Each element may be assigned an independent value for the Young's modulus, so each design is described by a 536-element vector $\{E_1, E_2, \ldots, E_{536}\}$ giving the Young's modulus for each hexagonal element.

For each design, the Comsol solver is used to calculate the response of the plate under a load per unit width of $P = 10$ N/m distributed uniformly over the top center hexagonal element. The resistance to bending is calculated based on the effective bending modulus of the composite plate, given by $E_{\text{bend}} = \frac{2L_x^3 P}{L_y^3 d}$, where d is maximum deflection just below the contact point. Under ideal beam theory, a monolithic plate with a uniform Young's modulus E would have $E_{\text{bend}} = E$ according to this expression. Therefore, the calculated E_{bend} of each mesostructure design is equivalent to the Young's modulus of the monolithic plate that would have the same bending resistance.

In order to capture the trade-off between maximizing the bending stiffness of the plate and minimizing density, each design is scored according to the objective function: $f = -\log(\frac{E_{\text{bend}}}{E_0}) + \frac{E_{\text{ave}}}{E_0}$. Here E_{ave} is the average value of the Young's modulus over the whole plate, which is assumed to be proportional to the total weight; E_0 is a constant that may be considered to loosely correspond to the target bending stiffness of the design. The first term of the objective function decreases as the resistance to bending increases, while the second term increases as the average modulus of the plate increases and therefore acts as a penalty based on the density of the design.

Optimization methods

As in the case of the graded cylinder described above, optimization of the plate is performed using simulated annealing to minimize the objective function f. Due to the large number of degrees of freedom present in this problem, the optimization is performed in two stages. In the first coarse optimization stage, the possible values of the Young's modulus for each hexagonal element are constrained to the set {3,
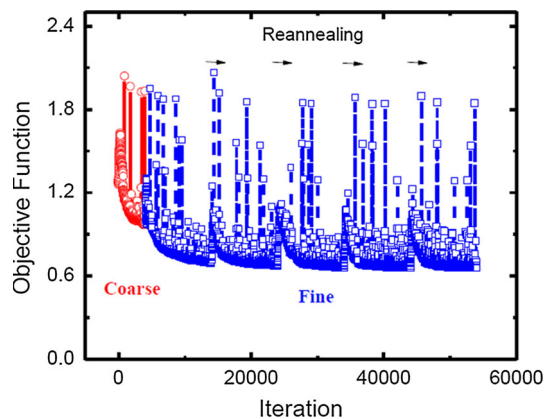
Figure 6 Plot of the objective function as a function of iteration number during simulated annealing, including the coarse and fine optimization steps.

30, 300} GPa, in order to quickly probe the design space to determine favorable regions of high and low density. The best solution from the coarse optimization is then used as the initial point for the second, fine optimization, for which the Young's modulus for each hexagonal element is permitted to take any of the values {3.0, 4.8, 7.5, 11.9 18.9, 30.0, 47.5, 75.4, 119.4, 189.3, 300} GPa. These values are selected to have log values evenly spaced between the softest and hardest materials in order to probe the widest range of effective properties.

The initial design for the full optimization is a monolithic plate with $E = 30$ GPa at all points. In each simulated annealing step, a random hexagonal element is chosen from the 536 in the design, and its Young's modulus is mutated randomly to one of the other allowed values. The objective function is then calculated for the mutated design, which is adopted as the seed for the next iteration with probability $P = \exp(-\frac{\Delta f}{T})$, where Δf gives the change in the objective function between the parent and mutated design. The coarse optimization is run for 4000 iterations, with an initial temperature $T_0 = 1$, which is decreased slightly with each iteration. The fine optimization is run for 50000 iterations, again with the initial temperature $T_0 = 1$, which is decreased slightly with each iteration, but restored to its initial value every 10000 iterations. This periodic reannealing procedure permits the design to escape from local minima more efficiently, while still allowing time to converge to a good local solution in between reannealing steps.

Optimization results

The change in the objective function over the course of the whole optimization process is shown in Fig. 6. The objective function is seen to decrease rapidly during the first 4000 iterations, corresponding to the coarse optimization. This results in the intermediate solution (upper figure in Fig. 7), with an objective function value of 0.97 relative to a starting value of 1.26 for the monolithic plate. Although the intermediate solution consists mostly of the initial material with $E = 30$ GPa, the coarse optimization step produces a design with clear segregation of the high-density material to a few critical areas adjacent to the contact points, as well as in the bottom center of the plate. At the same time, the low-density material is used in several places that are less important for determining bending stiffness, in particular the outer top corner, allowing for a decrease in the density penalty without overly compromising the bending stiffness. The intermediate solution also uses a substantial fraction of low-density hexagonal elements in the center of the plate, while retaining a scaffold of intermediate density material to provide structural support.

The subsequent 50000 iterations (in blue) shown in Fig. 6 are associated with the fine optimization stage, producing the final optimized design shown in the lower panel in Fig. 7. Owing to the reannealing process designed in the fine optimization, the objective function can be seen to increase rapidly every 10000 iterations, in which the temperature is increased to allow for a high probability of taking several uphill steps. Following each reannealing cycle, the objective function converges to a new lower value, as the design is locally relaxed to an optimum value. The final optimized design (lower panel in Fig. 7) shows a nearly smoothly graded structure, with a similar overall density distribution to the intermediate solution (upper panel), in particular prioritizing high-density and stiff materials at the contact points and along the bottom center of the plate, while decreasing the density on the top corners. The higher-density material also appears to be locally organized into linear chains, which would be expected to be more effective at providing structural support than a randomly distributed composite of equal density.

The objective function is further reduced from 0.97 by the intermediate solution to 0.66 by the final optimized design. The final optimized thin plate has
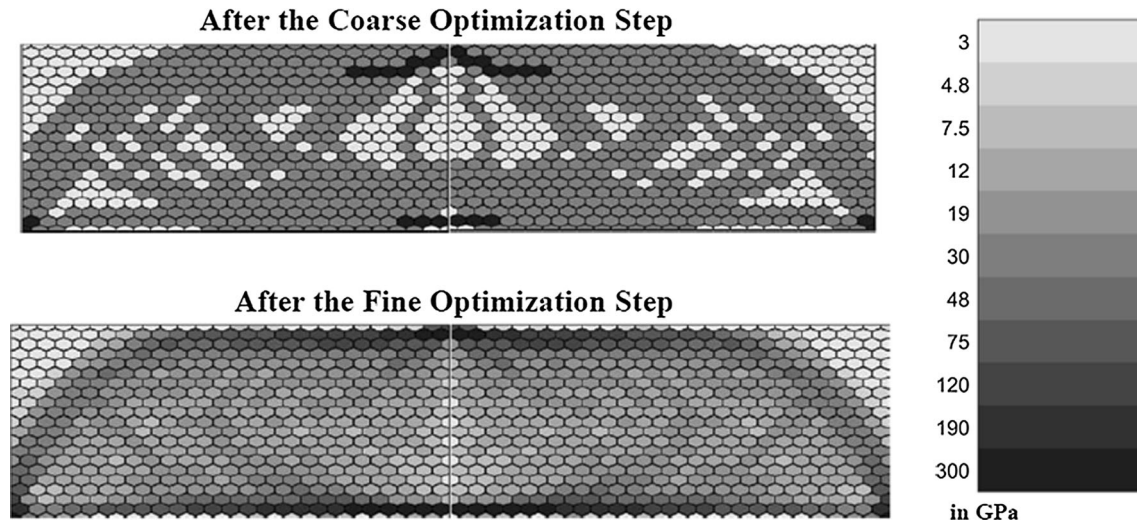
Figure 7 Optimal distribution of Young's modulus after the coarse optimization step (*the upper figure*) and after the fine optimization step (*the lower figure*).

a bending stiffness of 41.3 GPa and an average Young's modulus of 29.3 GPa in the optimized plate. To compare, a monolithic plate with the same average Young's modulus only has a bending stiffness of 22.5 GPa based on finite element modeling. To achieve the same bending stiffness, a monoclinic plate would require an average Young's modulus of 53.8 GPa (which is proportional to the total weight). Therefore, 2D mesostructure optimization in this example problem leads to an 83.6% increase in bending stiffness compared to a monoclinic plate with the same weight or a 83.6% reduction of the total weight compared to a monoclinic plate with the same bending resistance.

We have also repeated the above optimization procedure for the case of a more conventional binary topology optimization. With only the hardest ($E = 300$ GPa) and softest ($E = 3$ GPa) materials available to fabricate the plate, the objective function converges at 1.50 after 48000 cycles. To compare, with a range of materials available ($E = 3.0, 4.8, 7.5, 11.9$ $18.9, 30.0, 47.5, 75.4, 119.4, 189.3, 300$ GPa) in the above optimization problem, the optimal value of the objective function is 0.66. Apparently, mesostructure optimization that is enabled by mixing materials in additive manufacturing can lead to substantial improvement in mechanical performance as compared to a simple binary topology optimization.

Experimentally, such a voxel-specific mesostructured plate should be producible by multi-material fabrication. Using inkjet 3D printing with multiple

heads, for instance, Oxman and coworkers [10, 40, 41] have fabricated a design object with locally varying material stiffness by defining the material composition based on voxel resolution. Voxel-specific multi-material printing in hard inorganic materials remains a frontier area for experimental development, but it is hoped that the present simple demonstration may encourage more work in this direction, given the potentially large property benefits that may come from mesostructure optimization.

Conclusion and outlook

We offer two examples as simple illustrations of the large benefits possible through mesostructure optimization, i.e., the optimization of material structure and properties across the scale of an entire component, which becomes plausible thanks to multi-material additive manufacturing. Such optimization methods could present a rigorous approach to designing gradient materials as well as 2D and 3D digital materials, which has historically been highly constrained to material distribution profiles that either are arbitrary or result from manufacturing constraints [42]; with multi-material additive manufacturing, such constraints can be relieved and new levels of performance unlocked.

As demonstrated in the contact loading and the plate bending problems, mesostructure optimization is capable of rendering substantial efficiencies in

materials usage, weight savings, load-bearing capacity, and other figures of merit. In particular, our plate bending example suggests that multi-material mesostructure optimization can even outperform conventional topology optimization of monolithic materials. With this manuscript serving as the theoretical basis, multi-material additive manufacturing experiments present a direction for the future work of the present authors, to implement materials design through mesostructure optimization. Looking ahead, mesostructure optimization can also be applied to multi-physics applications [43], which may involve coupling between mechanical, thermal, electrical, chemical, and optical effects.

Acknowledgements

References

[1] Bourell DL, Leu MC, Rosen DW (2009) Roadmap for additive manufacturing: identifying the future of freeform processing. The University of Texas, Austin, Texas

[2] Gebhardt A (2012) Understanding additive manufacturing: rapid prototyping, rapid tooling, rapid manufacturing. Hanser Publications, Cincinnati

[3] Gibson I, Rosen DW, Stucker B (2010) Additive manufacturing technologies, SpringerLink (Online service). Springer, New York

[4] Hopkinson N, Hague RJM, Dickens PM (2006) Rapid manufacturing: an industrial revolution for the digital age. Wiley, Chichester

[5] Compton BG, Lewis JA (2014) 3D printing of lightweight cellular composites. Adv Mater 26:5930–5935

[6] Bauer J, Hengsbach S, Tesari I, Schwaiger R, Kraft O (2014) High-strength cellular ceramic composites with 3D microarchitecture. Proc Natl Acad Sci USA 111:2453–2458

[7] Smay JE, Gratson GM, Shepherd RF, Cesarano J, Lewis JA (2002) Directed colloidal assembly of 3D periodic structures. Adv Mater 14:1279–1283

[8] Hofmann DC, Roberts S, Otis R, Kolodziejska J, Dillon RP, Suh JO, Shapiro AA, Liu ZK, Borgonia JP (2014) Developing gradient metal alloys through radial deposition additive manufacturing. Sci Rep 4:5357

[9] Banerjee R, Collins PC, Bhattacharyya D, Banerjee S, Fraser HL (2003) Microstructural evolution in laser deposited compositionally graded α/β titanium-vanadium alloys. Acta Mater 51:3277–3292

[10] Oxman N, Keating S, Tsai E (2011) Functionally graded rapid prototyping, innovative developments in virtual and physical prototyping. In: Proceedings of the 5th international conference on advanced research in virtual and rapid prototyping, CRC Press, Taylor & Francis

[11] Bendsøe MP, Sigmund O (2003) Topology, optimization: theory, methods, and applications. Springer, Berlin

[12] Rozvany GIN (1997) Topology optimization in structural mechanics. Springer, Wien

[13] Bruns TE, Tortorelli DA (2001) Topology optimization of non-linear elastic structures and compliant mechanisms. Comput Methods Appl Mech Eng 190:3443–3459

[14] Bureerat S, Limtragool J (2006) Performance enhancement of evolutionary search for structural topology optimisation. Finite Elem Anal Des 42:547–566

[15] Lamberti L (2008) An efficient simulated annealing algorithm for design optimization of truss structures. Comput Struct 86:1936–1953

[16] Moita JMS, Correia VMF, Martins PG, Soares CMM, Soares CAM (2006) Optimal design in vibration control of adaptive structures using a simulated annealing algorithm. Compos Struct 75:79–87

[17] Sigmund O (1997) On the design of compliant mechanisms using topology optimization. Mech Struct Mach 25:493–524

[18] Suzuki K, Kikuchi N (1991) A homogenization method for shape and topology optimization. Comput Methods Appl Mech Eng 93:291–318

[19] Rozvany GIN (2009) A critical review of established methods of structural topology optimization. Struct Multidiscip Optim 37:217–237

[20] Adams BL, Kalidindi S, Fullwood DT (2013) Microstructure sensitive design for performance optimization. Butterworth-Heinemann, Waltham

[21] Torquato S (2010) Optimal design of heterogeneous materials. Annu Rev Mater Res 40:101–129

[22] Torquato S (2002) Random heterogeneous materials: microstructure and macroscopic properties. Springer, New York

[23] Johnson OK, Schuh CA (2013) The uncorrelated triple junction distribution function: towards grain boundary network design. Acta Mater 61:2863–2873

[24] Cross SR, Woollam R, Shademan S, Schuh CA (2013) Computational design and optimization of multilayered and functionally graded corrosion coatings. Corros Sci 77:297–307

[25] Suresh S, Mortensen A (1998) Fundamentals of functionally graded materials: processing and thermomechanical

behaviour of graded metals and metal–ceramic composites. IOM Communications Ltd, London

[26] Mortensen A, Suresh S (1995) Functionally graded metals and metal–ceramic composites: part 1 processing. Int Mater Rev 40:239–265

[27] Suresh S, Mortensen A (1997) Functionally graded metals and metal–ceramic composites: part 2 thermomechanical behaviour. Int Mater Rev 42:85–116

[28] Johnson KL (1985) Contact mechanics. Cambridge University Press, Cambridge

[29] Ashby MF (2005) Materials selection in mechanical design, 3rd edn. Butterworth-Heinemann, Amsterdam

[30] Yang X-S (2014) Nature-inspired optimization algorithms. Elsevier, London

[31] Seidel R et al (2016) Ultrastructural and developmental features of the tessellated endoskeleton of elasmobranchs (sharks and rays). J Anat 229:681–702

[32] Gibson LJ (2012) The hierarchical structure and mechanics of plant materials. J R Soc Interface 9:2749–2766

[33] Dixon PG, Gibson LJ (2014) The structure and mechanics of Moso bamboo material. J R Soc Interface 11:20140321

[34] Balla VK et al (2007) Compositionally graded yttria-stabilized zirconia coating on stainless steel using laser engineered net shaping (LENS). Scripta Mater 57:861–864

[35] Balla VK et al (2009) Fabrication of compositionally and structurally graded Ti–TiO$_2$ structures using laser engineered net shaping (LENS). Acta Biomater 5:1831–1837

[36] Wilson J, Shin YC (2012) Microstructure and wear properties of laser-deposited functionally graded Inconel 690 reinforced with TiC. Surf Coat Technol 207:517–522

[37] Vaezi M et al (2013) Multiple material additive manufacturing—part 1: a review. Virtual Phys Prototyp 8:19–50

[38] Tammas-Williams S, Todd I (2016) Design for additive manufacturing with site-specific properties in metals and alloys. Scripta Materialia. doi:10.1016/j.scriptamat.2016.10.030

[39] Liu W, DuPont JN (2003) Fabrication of functionally graded TiC/Ti composites by laser engineered net shaping. Scripta Mater 48:1337–1342

[40] Stratasy website. http://www.stratasys.com/materials/polyjet/digital-materials

[41] Doubrovski EL et al (2015) Voxel-based fabrication through material property mapping: a design method for bitmap printing. Comput Aided Des 60:3–13

[42] Suresh S (2001) Graded materials for resistance to contact deformation and damage. Science 292:2447–2451

[43] Sigmund O (2001) Design of multiphysics actuators using topology optimization—part I: one-material structures. Comput Methods Appl Mech Eng 190:6577–6604